Article

Influence of Micro-Textures on Cutting Insert Heat Dissipation

José Rosas [1], Hernani Lopes [1,*], Bruno Guimarães [2], Paulo A. G. Piloto [3], Georgina Miranda [2,4], Filipe S. Silva [2] and Olga C. Paiva [1]

1　Centre for Research & Development in Mechanical Engineering-Department of Mechanics (CIDEM-DEM/ISEP), School of Engineering, Polytechnic Institute of Porto, Rua Dr. Roberto Frias, 712, 4200-465 Porto, Portugal; 1160512@isep.ipp.pt (J.R.); omp@isep.ipp.pt (O.C.P.)
2　Center for Microelectromechanical Systems (CMEMS-UMinho), University of Minho, Campus de Azurém, 4800-058 Guimarães, Portugal; brunopereiraguimaraes@hotmail.com (B.G.); gmiranda@ua.pt (G.M.); fsamuel@dem.uminho.pt (F.S.S.)
3　Instituto Politécnico de Bragança, Department of Applied Mechanics, Campus de Santa Apolónia, 5300-253 Bragança, Portugal; ppiloto@ipb.pt
4　CICECO, Aveiro Institute of Materials, Department of Materials and Ceramic Engineering, University of Aveiro, 3810-193 Aveiro, Portugal
*　Correspondence: hml@isep.ipp.pt

Abstract: Metal machining is one of the most important manufacturing processes in today's production sector. The tools used in machining have been developed over the years to improve their performance, by reducing the cutting forces, the friction coefficient, and the heat generated during the cutting process. Several cooling systems have emerged as an effective way to remove the excessive heat generated from the chip-tool contact region. In recent years, the introduction of nano and micro-textures on the surface of tools has allowed to further improve their overall performance. However, there is not sufficient scientific data to clearly show how surface texturing can contribute to the reduction of tool temperature and identify its mechanisms. Therefore, this work proposes an experimental setup to study the tool surface characteristics' impact on the heat transfer rate from the tools' surface to the cooling fluid. Firstly, a numerical model is developed to mimic the heat energy flow from the tool. Next, the design variables were adjusted to get a linear system response and to achieve a fast steady-state thermal condition. Finally, the experimental device was implemented based on the optimized numerical model. A good agreement was obtained between the experimental tests and numerical simulations, validating the concept and the implementation of the experimental setup. A square grid pattern of 100 μm × 100 μm with grooves depths of 50, 100, and 150 μm was introduced on cutting insert surfaces by laser ablation. The experimental results show that there is a linear increase in heat transfer rate with the depth of the grooves relatively to a standard surface, with an increase of 3.77% for the depth of 150 μm. This is associated with the increase of the contact area with the coolant, the generation of greater fluid turbulence near the surface, and the enhancement of the surface wettability.

Keywords: cutting insert; micro-textures; heat transfer rate; experimental device

1. Introduction

Machining is a process that has been used from ancient times to the present day for producing a wide variety of objects, through the controlled removal of material [1]. Today's metal machining industry's competitive market demands high productivity and quality at lower costs, especially for turning and milling operations. This is normally achieved by choosing the optimal machining strategies and selecting higher-performing tools. A strong effort has been made in developing new tools intended for machining heat-resistant super metal alloys (HRSA), with the introduction of specific tungsten-carbine metal alloys, surface coatings, and optimized tool geometry [2–5]. A typical limitation in machining HRSA, compared to common materials, is the superior heat generated during the cutting

process, which must be extracted from the cutting zone using conventional or more advanced cooling techniques [6]. Several cooling methods have been attempted to reduce the temperature, namely high-pressure cooling, minimum lubrification quantity, compressed air cooling, heat pipe cooling, cryogenic cooling, and internal cooling [7–11]. A new line of research is focused on combining the micro-textures with high-pressure cooling to increase the thermal dissipation in turning and milling operations [3,4,12,13]. The introduction of micro-textures on the cutting inserts has been explored to increase lubrication efficiency and, thereby, reduce to the minimum the amount of cutting fluid [14]. An extensive survey on textured cutting insert performance, for different machining processes, texturing methods, cutting insert materials, tool coatings, workpiece metal materials, and lubricant conditions, can be found in [15]. The nano and micro surface texturing are introduced near the tool's cutting edge to reduce cutting forces, friction, tool wear, surface roughness, machining temperatures, adhesion of particles, and to extend tool life [2,15–17]. The nano textures reduce the chip adhesion when machining aluminum, while the combination of nano- and micro-textures reduces built-up edge formation when machining carbon steel alloys [15]. Other studies show that the combination of nano- with micro-textures is also effectively reducing the adhesion of aluminum to the tool, for dry and lubricated conditions [18]. A review of the mechanisms behind improving cutting performance through the application of surface coatings, high-energy beam treatments, and surface texturing is presented in [19]. It's mentioned the purpose of texturing is to improve the tribological properties of the cutting insert surface, by enhancing the lubrication at the chip-tool interface, trapping the abrasive particles, reducing the contact area, and promoting chip evacuation [19]. Tools abrasion by the wear particles can benefit from the trapping mechanism of the particles due to the microchannels. These can also reduce the surface tension, resulting in increased cutting fluid spreading speed and the surface wettability, improvement in lubrication effect, and the overall tool performance [15,20–24]. Round grooves are the most used textures due to their simple manufacturing process. These continuous channels have the advantage of conducting cutting fluid faster than round dimples, leading to a smaller contact length between the chip and the tool [25,26]. The combination of coatings with nano-textures has also allowed improving the cutting performance and surface finish of high-hardness steels in turning operations [27]. Micro-pools of cutting fluid contribute to the decrease of the contact area between the chip and the tool, leading to a reduction of friction coefficient and, therefore, the cutting forces [26,28]. Some studies reported that the improvement of cutting performance depends on texture dimensions, shape, and orientation [19]. The grooves' orientation parallel to chip flow improves the cutting performance [26,29–31]. However, these textures must be located away from the cutting edge to preserve their integrity, being the minimum distance function of the thickness of the uncut chip [24]. The major amount of research is focused on the reduction of cutting forces and friction coefficient. The decrease in cutting temperature and the increase in the tool's life is treated as a consequence of these improvements. On the other hand, the enhancement of heat extraction from the chip-tool contact zone has become a new research field in the last years. The theoretical assumption is that surface textures promote a more turbulent flow of cutting fluid, resulting in a significant increase in the cooling process [26]. The effect of thermal contact resistance between the cutting insert and the assembly parts was also investigated numerically [31]. The introduction of silicone oil to remove the air gap between the cutting insert and the holder allowed for a decrease in the tool's maximum temperature from 913.72 °C to 818.93 °C [31]. Some works address the interaction between coolant and the cutting insert by studying the drop spreading behavior on WC-Co cutting tools surface of the water and machining cutting fluid [2–4,12,13,23,31–33]. The mechanism of interaction between the coolant and the surface texture is still not fully understood due to the simultaneous action of several physical phenomena and, from an experimental point of view, several limitations inhibit temperature monitoring in the chip-tool contact region. The effectiveness of cooling in the tool-chip contact region is normally evaluated indirectly by measuring tool wear on the rake face, the cutting forces, the remote temperature, and

chip morphologies, in the case of experimental tests [2–4,13,32]. For the case of numerical simulations of the cutting process using the Finite Element Method, the temperature is directly computed [12,13,31,33]. There have been a few attempts to measure the temperature in the contact region, but the technique is either very restrictive concerning workpiece materials or the measurement includes regions beyond the chip-tool contact [34,35]. Even with the technological advances of recent years, it remains a great challenge to accurately measure the temperature in this region. The main techniques applied to temperature measurement near the chip-tool contact region are based on the physical principle of conduction and radiation [36,37]. The thermocouples and thermal paints belong to the conduction group, whereas the optical infrared laser pyrometer and thermographic cameras fit into the radiation [38]. However, in the presence of cooling fluid, the temperature measurement is limited to conduction techniques since the fluid can drastically affect thermal radiation. Also, it is not advisable to mount a built-in thermocouple close to the tip, as this can lead to an increase in stress concentration and lower the tool's life [39]. Another limitation encountered when performing cutting operations is the difficulty in controlling the parameters that can influence the temperature generated in the chip-tool interface, namely: material properties, chip evacuation, tool wear, micro-texturing filing, material adhesion, coolant direction/pressure, and more [2,28,40].

The present work is part of broader research that seeks to improve cutting tool performance by increasing the heat transfer rate, achieved through the incorporation of surface micro-textures. Its implementation has the objective of increasing the contact area between the surface and cooling, promoting a greater turbulent flow of the fluid near the surface and enhancing the surface wettability. The effectiveness of micro-textures can only be evaluated through experimental tests. Therefore, this work aims to develop an experimental device capable of accurately measuring the heat transfer rate from the cutting insert surface to the coolant in a very controlled environment. The device was conceived to simulate the heat transfer phenomena from the tool to the cooling fluid during the cutting operation, being developed using a computer-aided design (CAD) tool. It is followed by a numerical study using commercial software Ansys Fluent® (Washington County, PA, USA) to evaluate the overall sensitivity and thermal stability. The device response linearity is evaluated by measuring the heat transfer rate for different levels of input power, which are compared with a fine-tuned FVM model. The effectiveness of the device is assessed based on the experimental tests. Finally, three different surface micro-textures are analyzed and compared to a standard surface tool, to verify their influence on the heat transfer rate.

2. System Design and Implementation

This section presents the system concept, the CAD model, thermal-mechanical numerical analysis, and the experimental device implementation.

2.1. Concept

Every experimental test deals with a set of variables that need to be monitored to get trustworthy results. This requires the development of an experimental setup where all the variables are controlled and the physical quantities measured, using proper instrumentation. However, the temperatures generated during the machining process are dependent on the chip geometry, mechanical and thermal properties of the material, tool material microstructure, and tool wear, which are impossible to control during the entire process [17,35]. Therefore, the heat transfer quantification due to the introduction of micro-textures becomes a challenge by performing machining tests. To overcome these limitations, a specific experimental setup is developed to mimic the heat transfer during the cutting process and also allow its quantification. This is composed of an internal closed circuit for the flow of the cooling fluid, an input power control system, and a system for monitoring the inlet and outlet fluid temperatures. The design of this device required the construction of a numerical model to analyze the fluid flow, quantify the heat extraction from the cutting insert surface, study the response and evaluate the system thermal stability. Other relevant

characteristics were also considered in the design phase, namely: the manufacturing process, instrumentation, flexibility, cost, repeatability, simplicity of the procedure, and the time required for the analysis.

2.2. CAD Modelling

The CAD model was developed in SolidWorks® (Waltham, MA, USA) to reproduce the geometry and the heat transfer from the cutting insert surface to the cooling fluid that occurs during the machining process. The final model was found after a few iterations taking into consideration the objectives and the constraints of the problem. Figure 1 depicts the final model with the identification of its main components. The heat flux is introduced into the cutting insert lateral faces, the coolant fluid is guided over its upper surface and the inlet and outlet temperatures are monitored to quantify the heat transfer rate. The main body (1) has the purpose of supporting and fixing all components, with the additional function of providing thermal inertia equivalent to a tool holder. The support seat (2) includes slots to allow the installation of two thermocouples to monitor the main body temperature and four thermocouples to monitor the lower surface temperature of the cutting insert (3). The main stud (4) is used to guide and fix the support seat, the insert, and the top chamber (5) to the main body (1). The heat power is laterally introduced into the insert by its contact with the two heat sources (6). Each heat source is capable of generating 200 W, through the mounting of 4 resistive elements of 50 W each (7), making a total power generation of 400 W.
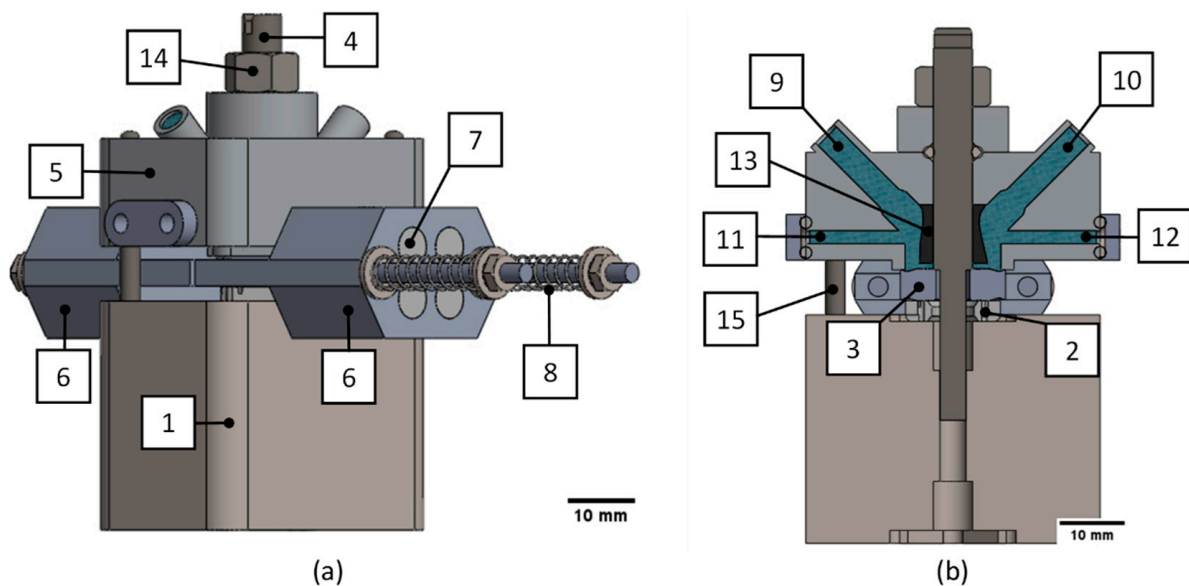
Component	Name	Component	Name
1	Main body	9	Inlet channel
2	Support seat	10	Outlet channel
3	Cutting insert	11	Inlet thermocouple channel
4	Main stud	12	Outlet thermocouple channel
5	Top chamber	13	Core
6	Heat sources	14	Nut
7	Resistive element	15	Guide pin
8	Springs		

Figure 1. CAD model with components identification: (**a**) full assembly; (**b**) middle cross-section.

To enable the assembly of these elements and ensure a good heat transfer, the heat source elements are made of aluminum and possess four reamed holes. The compression force generated by the helicoidal springs (8) mounted on the two threaded rods, guarantees permanent pressure between the cutting insert and heat source surfaces, and minimizes the stresses created by the thermal expansion of the materials. The top chamber includes the coolant inlet and outlet channels (9) and (10), respectively, and two instrumentation channels, (11) and (12), for the temperature gradient measurement, needed for the evaluation of the heat transfer rate. In the center of the chamber, a core element (13) was added to promote the uniform coolant fluid flow over the entire top surface of the cutting insert. The top chamber sealing is ensured by the compression force against the insert cutting edge, produced by the tightening of the nut (14), located on the top of the main stud (4). The two guide pins (15) ensure alignment between the main body (1) and the top chamber (3).

2.3. Numeric Study

The numerical thermal-fluid-solid coupling study is conducted to investigate the proposed device's effectiveness and linearity, by using a pressure-based solver from ANSYS-Fluent®, solving the momentum, continuity, and energy equations. This involved determining the optimal dimensions of the internal fluid flow channels, maximizing the coolant temperature gradient, between inlet and outlet, and obtaining a uniform distribution of the cutting insert surface temperature, keeping its top surface below 100 °C to avoid latent heat absorption. The final dimensions of the flow channels and the core geometry were obtained after a few iterations.

The average and standard deviations values for mass density and thermal properties of the materials, considered for the numerical simulations, are indicated in Table 1. For the analysis' sake of simplicity, the thermal conductivity of the materials is assumed to be constant and independent of the temperature.

Table 1. Materials mass density and thermal properties.

Component	Material	Mass Density [kg/m^3]	Specific Heat [J/kg.K]	Thermal Conductivity [W/m.K]
Main body	AISI 1010 Steel	7849.80 ± 50.00	442.63 ± 20.00	56.59 ± 6.00
Top chamber	Aluminium 6082-t6	2699.80 ± 30.00	899.82 ± 18.00	171.97 ± 3.00
Heat sources	Aluminium 6082-t6	2699.80 ± 30.00	899.82 ± 18.00	171.97 ± 3.00
Cutting insert	WC-Co 90-10	14,550.00 ± 150.00	209.00 ± 4.00	89.50 ± 3.50
Support seat	WC-Co 90-10	14,550.00 ± 150.00	209.00 ± 4.00	89.50 ± 3.50
Main stud	AISI 1015	7849.80 ± 50.00	442.63 ± 20.00	52.02 ± 2.00
Nut	AISI 1015	7849.80 ± 50.00	442.63 ± 20.00	52.02 ± 2.00
Core	PET-G	1339.10 ± 50.00	1199.00 ± 50.00	0.17 ± 0.0065
Guide pin	AISI 304 Stainless Steel	7954.30 ± 105.00	473.62 ± 20.00	14.92 ± 1.50
Resistive element	AISI 304 Stainless Steel	7954.30 ± 105.00	473.62 ± 20.00	14.92 ± 1.50

The numerical simulation requires the knowledge of real thermal properties to achieve an effective and reliable solution. This involves the selection of the fluid thermal properties, the heat power input, coolant fluid mass flow rate, the initial temperatures, and the definition of the thermal boundary conditions. Given that the water is the basis of the commonly used cutting fluids, about 95%, its thermal properties are assumed for the numerical simulations. The heat power generation of 93.07 MW/m^3 was defined for each resistive electric element to simulate the electric input power of 50 W. A constant fluid mass flow rate of 15.6 g/s was defined to avoid exceeding the specified temperature limit of 100 °C at the top insert surface. The inlet water temperature was considered constant at 15.2 °C and the room temperature at 20.3 °C. Natural convection plays a key role in the temperature distribution throughout the device. The average value convection coefficient of 25 W/m^2.K was equally assumed for all the surfaces and thermal conductance of 11,000 W/m^2.K was considered between all components [41]. The values of natural

convection coefficient and thermal conductance were later fine-tuned to reproduce the experimental device response. The final values were obtained by applying the heuristic method. After a few iterations, a new convection coefficient of 10 W/m^2.K was considered for the main body (1) and 20 W/m^2.K for the support seat (2), main stud (4), top chamber (5), and nut (14). The thermal conductance final values between the top chamber (5), and the cutting insert (3) of 67,467 W/m^2.K, between the heat sources (6) and the cutting insert (3) of 6325 W/m^2.K, and 20,240 W/m^2.K between the cutting insert (3) and the support seat (2). The remaining values were kept unchanged.

The polyhedron mesh of 2,448,604 elements is shown in Figure 2. This was initially generated in Ansys Workbench as tetrahedron mesh and later converted using Fluent tools. A convergence study was carried out to define the proper mesh size. Five inflation layers were specified to properly describe the thermal and flow boundary condition effects. Numerical simulations were conducted for a steady regime by considering the previously described mesh and values of convection coefficients and thermal conductance, and the mass density and thermal properties values of the materials presented in Table 1. A constant mass flow rate of 15.6 g/s of water was considered for all the simulations.
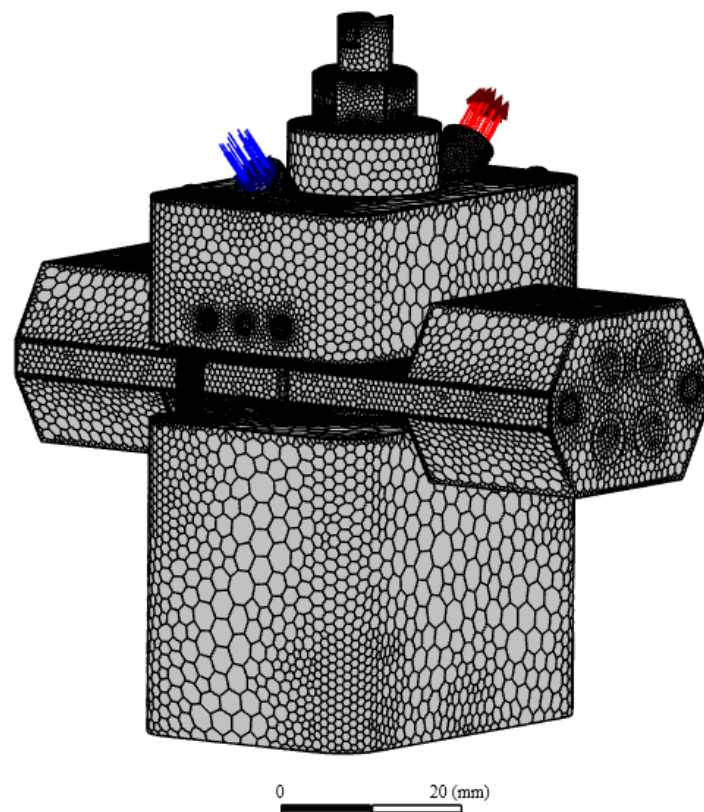

Figure 2. The model with polyhedron mesh, use in numerical simulations.

Figure 3 presents the temperature distribution of the cross-section and internal fluid flow lines, for the steady-state condition. In the cross-section is observed that the temperature of the cutting insert is lower than the heat sources, which is justified by the contact resistance and heat transfer to the fluid. The flow lines analysis also reveals a uniform path distribution over the top surface of the insert, as well as an increase in the fluid temperature from inlet to outlet.
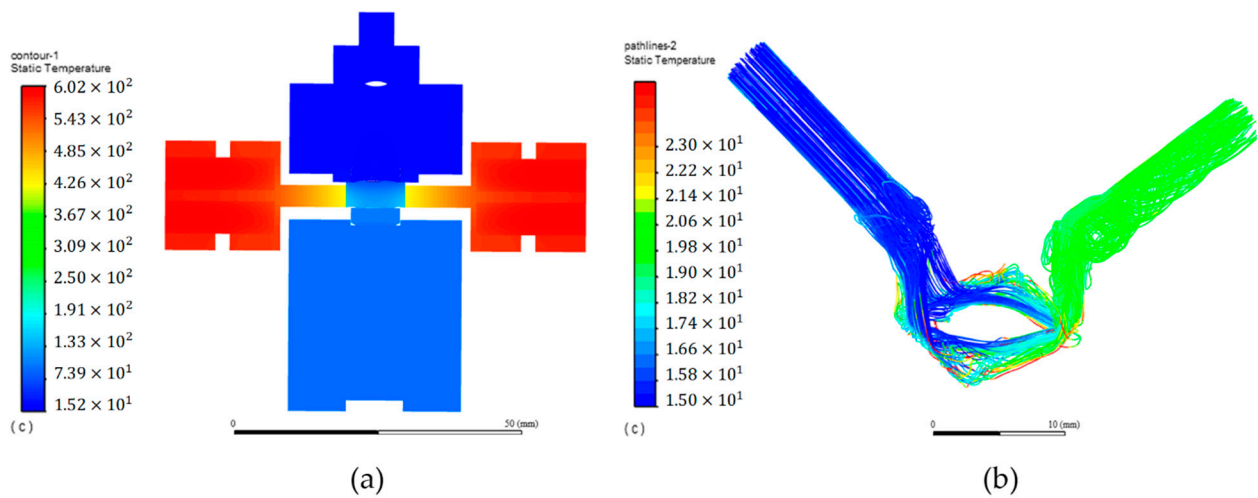
Figure 3. Temperature representation for steady-state condition: (**a**) model cross-section; (**b**) fluid flow lines.

The quantification of the heat transfer rate from the insert top surface to the fluid can be determined by measuring the fluid temperature differences between the inlet and outlet channels. However, the fluid temperature is not the same along the channels and, thus, the accuracy of the results strongly depends on the locations of the measurements. The position selection is not straightforward, since the stabilization of the fluid temperature tends to occur far from the cutting insert, see Figure 1, where the influence of heat transfer from the top chamber to fluid is more prevalent. Therefore, the selection of the best locations will result from the balance between the minimum distance to the cutting insert and the region where is achieved a reasonable fluid temperature stabilization. These were found by analyzing the fluid temperatures in the numerical model, being the most suitable locations for measuring the inlet (T1) and outlet (T2) temperatures identify in Figure 4.
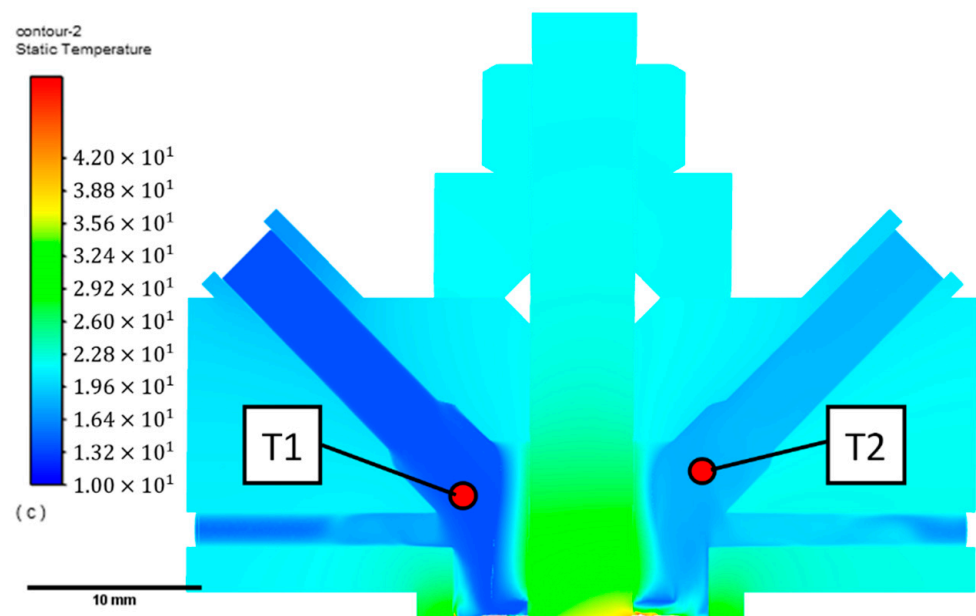

Figure 4. The best locations for measuring the fluid inlet and outlet temperatures.

Assuming a constant heat input power, a steady-state mass flow rate, a negligent kinetic and potential energies, and the work interaction, the heat transfer rate $\dot{Q}$ can be given by [40],

$$\dot{Q} = \dot{m}.c_p.\Delta T \quad [W] \tag{1}$$

where $\dot{m}$ is the mass flow rate in [kg/s], c_p is the specific heat at constant pressure in [J/kg.K], and ΔT is the temperature gradient, between the inlet T1 and outlet T2 express in [K]. The water mass density and thermal properties defined for numerical simulations were the following: mass density of 998.2 kg/m^3, specific heat of 4187 J/kg.K, thermal conductivity of 0.6 W/m.K, and dynamic viscosity of 0.001 kg/m.s.

From the numerical simulations and by considering four input power levels, the heat transfer rate was determined. This involves the measurement of the inlet and outlet fluid temperatures at locations identified in Figure 4 and the application of Equation (1). The measured temperatures, the mass flow rate, and the correspondent heat transfer rate for the input power of 100, 200, 300, and 400 W are presented in Table 2.

Table 2. Numerical thermal results for different input power levels.

Input Power [W]	T1 [°C]	T2 [°C]	ΔT [°C]	Mass Flow Rate [g/s]	Heat Transfer Rate [W]
100	15.22	16.39	1.17	15.6	76.41
200	15.25	17.57	2.32	15.6	151.29
300	15.27	18.73	3.46	15.6	226.09
400	15.29	19.88	4.59	15.6	299.65

The values in Table 2 show a linear trend between heat transfer rate and the input power. Also, is observed a high efficiency of heat transfer to the fluid, corresponding to about 75% of the input power. In detail, the inlet temperature T1 presents a slight increase with the input power, which is related to the fluid preheating by the top chamber. The same effect is expected for the fluid outlet temperature T2, being aggravated with the distance of the measurement points to the cutting insert. This means the compound effect will result in a slight overestimation of the heat transfer rate.

2.4. Experimental Device Description and Assembly

The main components of the experimental device were manufactured using a Computer Numerical Control (CNC) machine and the small parts using conventional machining processes, being the selected materials identified in Table 1. The core in PET-G presents a complex geometry, for this reason, was produced using Fused Deposition Modeling (FDM), an extrusion-based 3D printing. All the components used to build the experimental device are laid out in Figure 5a and the main steps for its assembly are shown in Figure 5b–d.

The location of the thermocouples for measuring the inlet (T1) and outlet (T2) temperature of the fluid are shown in Figure 5a. In Figure 5b is visible the insert seat with four thermocouples (T3–T6), to monitor the temperature on the cutting insert base, and two thermocouples (T7–T8), to monitor the main body temperature. The cutting insert assembly, the heat sources, and the 8 resistive electric elements are visible in Figure 5c. Two more thermocouples (T9–T10) are used to monitor the temperature in the insert-heat sources interface, located near the cutting insert tip. The complete assembly of the device with the volumetric pump is presented in Figure 5d. This last picture also shows the pipes connections from the volumetric pump to the inlet channel and from the outlet channel to the sink, as well as the thermocouples wires connected to the signal acquisition system of National Instruments®, model NI 9213. Water is used as coolant fluid due to the large amount needed to perform experimental tests. The freshwater is pumped at a constant flow rate into the inlet channel of the device, where the temperature is measured by thermocouple T1. The water carries on to the upper surface of the cutting insert, where most of the heat transfer occurs. In the outlet channel, the water temperature is measured by thermocouple T2, and then it is expelled. A k-type thermocouple was selected for the temperature

measurement at ten different points of the experimental device. These were manufactured by welding the hot junction tip in an inert atmosphere with suitable equipment, being later calibrated using the PREZYS T-25N equipment. The thermocouples were mounted into the device using suitable silicones and adhesive tapes, selected according to the restrictions and operating conditions.
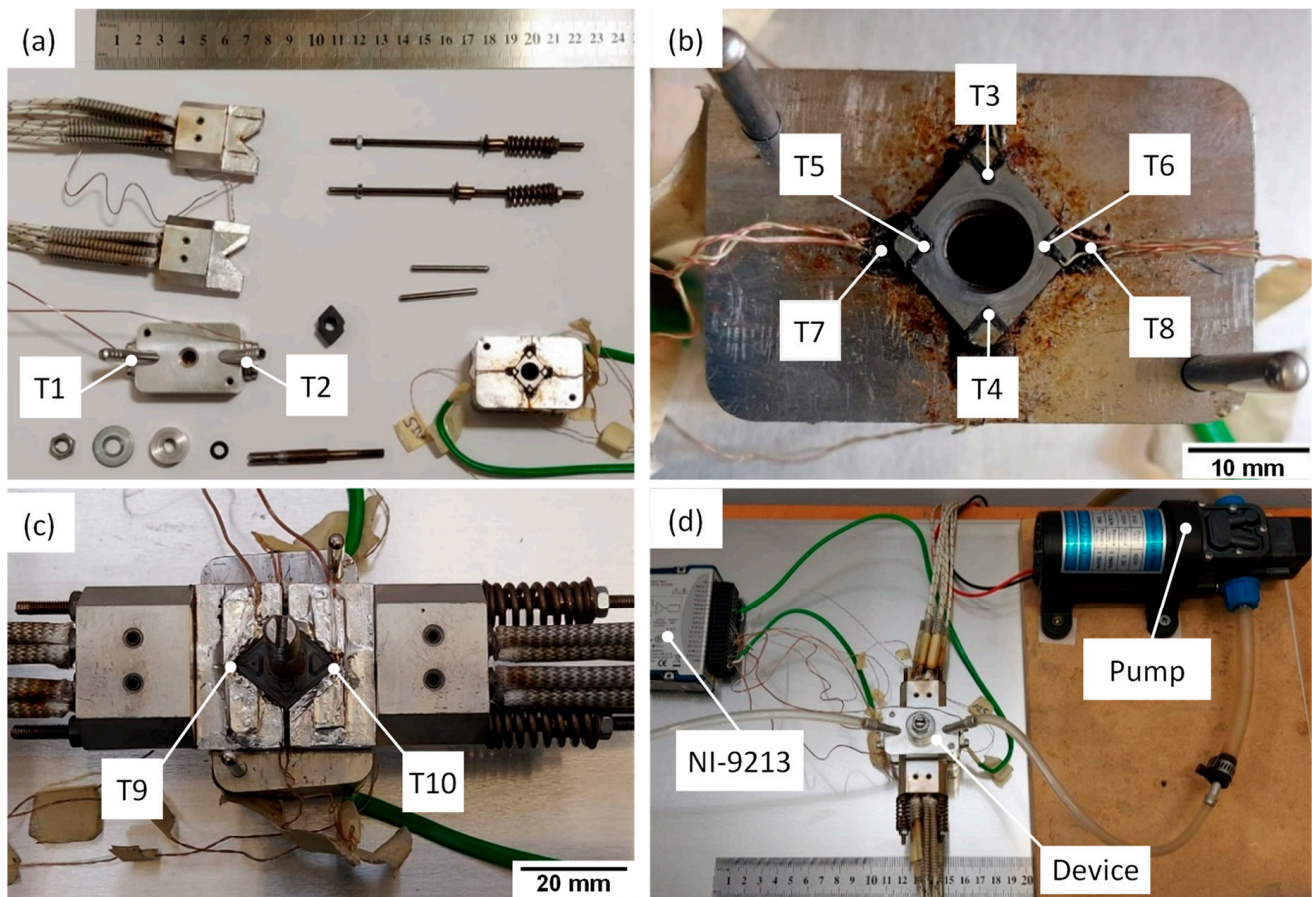

Figure 5. Experimental device images: (**a**) laid out components; (**b**–**d**) assembly main steps.

3. Experimental Study

The following subsections present the implementation of surface micro-textures, the description of the measurement procedure, the experimental device validation, and the results and discussion of the heat transfer rate for cutting inserts with different micro-textures.

3.1. Surface Micro-Textures Implementation

The main motivation for introducing micro-textures on cutting insert surfaces is their potential contribution to reducing the cutting insert temperature. The best way of creating custom surface textures is through laser ablation of WC-Co green compact inserts. Contrarily to sintered WC-Co, this method minimizes the problems of creating spatter, heat-affected zones, and microcracks, with the additional advantages of improving machining efficiency and reducing cost [21,42]. WC-10 wt.% Co green compacts inserts were pressed at Palbit S.A. company. The surface micro-textures were created by laser surface texturing, using an Nd: YAG laser, being the square grid pattern produced in accordance with the work previously reported in the literature [43]. The green inserts were then post-dewaxing and sintering, according to Palbit S.A. specifications [43]. In Figure 6, the images of four sintered WC-Co inserts, model CNMG 120408-GS are presented, and the respective magnified view of the surface

micro-textures. One has a standard surface topology, and the three others have a square grid pattern of 100 μm × 100 μm with an average depth of 50, 100, and 150 μm, being, respectively, designated by Grid depth 1, Grid depth 2, and Grid depth 3. The experimental tests were performed with uncoated inserts to avoid interference in the heat transfer rate assessment.
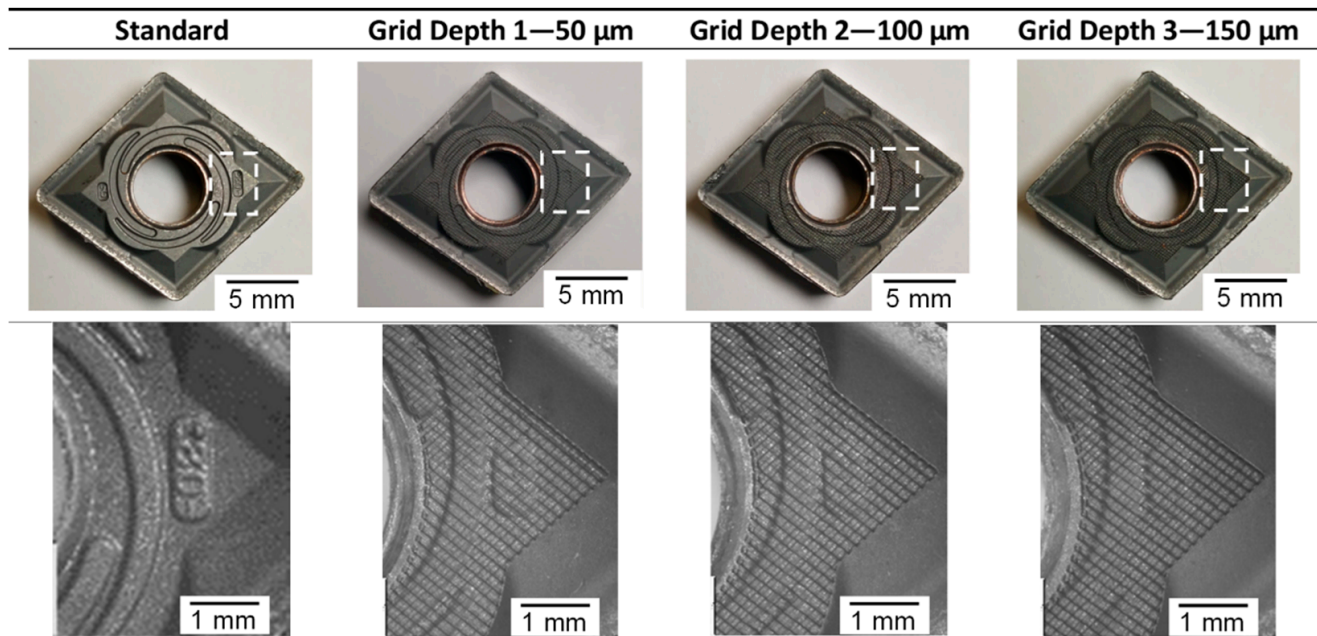

Figure 6. Cutting inserts images and the magnified view of their surface micro-textures.

3.2. Measurement Procedure

A procedure was defined to guarantee good results and the repeatability of experimental tests. This includes the cutting insert installation sequence, the measurement procedure of temperature and mass flow rate, the power supply connections to the resistive element, and the temperature analysis. A set of auxiliary elements are used to guarantee the positioning of different cutting inserts during the system assembly. The same clamping force is applied during the assembly, by controlling the tightening torque with a torque wrench. The power supply stability and the input power balance are important for the quality of the results. The maximum input power requirement of 400 W led to the installation of two power supplies, each capable of providing more than 200 W. The matching pair of resistive elements were connected to the same power supply channel, and each of them was mounted on a different heat source. This ensures the input power balance and improves the system's thermal stability. The temperature signals are acquired through the NI-9213 thermocouple module, in high-resolution mode, which corresponds to a measurement accuracy of <0.02 °C. After the system reaches the steady-state thermal condition, see Figure 7, the temperature is taken within a five-minute interval and its average value is used to compute the heat transfer rate. The mass flow rate is evaluated by weighting the amount of water captured in a reservoir during this period. This is followed by the cool-down phase, which begins by turning off the power supplies. This can be accelerated by leaving the freshwater flow during this phase, which allows reducing the time for starting a new experimental test.
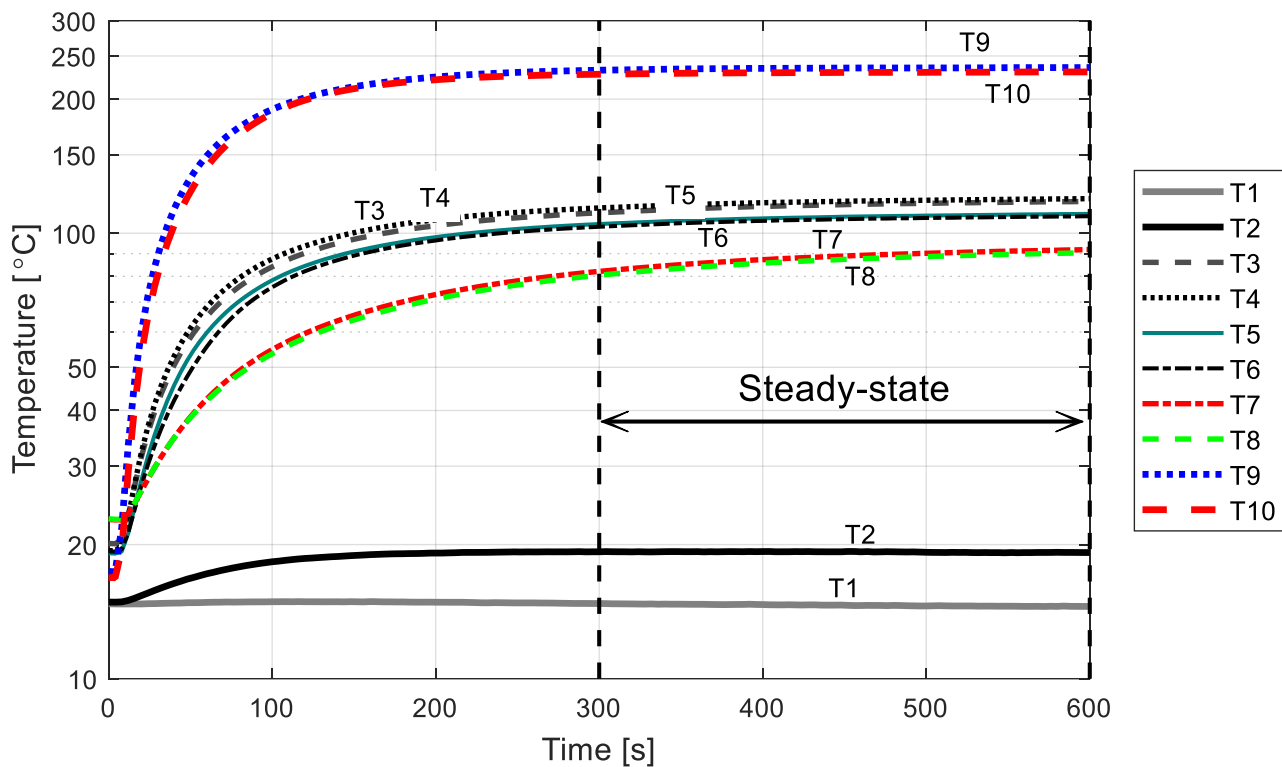
Figure 7. Temperature-time evolution during the heating phase, for the input power level of 400 W.

3.3. Experimental Device Validation

Several tests were performed to evaluate the implemented experimental device. This involved the measurement of the inlet T1 and outlet T2 temperatures and the evaluation of the respective heat transfer rate for standard cutting inserts, by considering the input power levels of 100, 200, 300, and 400 W. Three experimental tests were made for each input power level, and the heat transfer rate was determined by Equation (1), in which the specific heat value of 4187 J/kg.K was considered. The averages and the standard deviation values (Avg $\pm$ SD) for the inlet and outlet temperatures, the temperature gradient, the mass flow rate of water, and the heat transfer rate, for each input power level, are presented in Table 3.

Table 3. Experimental thermal results for different input power levels.

Input Power [W]	T1 [°C]	T2 [°C]	ΔT [°C]	Mass Flow Rate [g/s]	Heat Transfer Rate [W]
100	15.68 $\pm$ 0.11	16.89 $\pm$ 0.10	1.21 $\pm$ 0.01	15.64 $\pm$ 0.0481	79.16 $\pm$ 0.23
200	15.74 $\pm$ 0.11	18.04 $\pm$ 0.11	2.29 $\pm$ 0.01	15.58 $\pm$ 0.0337	149.67 $\pm$ 0.41
300	15.50 $\pm$ 0.35	18.91 $\pm$ 0.34	3.40 $\pm$ 0.01	15.57 $\pm$ 0.0144	221.87 $\pm$ 0.24
400	15.62 $\pm$ 0.32	20.19 $\pm$ 0.33	4.57 $\pm$ 0.01	15.64 $\pm$ 0.0481	299.16 $\pm$ 0.40

By comparing the heat transfer rate results in Table 3 with the ones in Table 2, one can confirm a high level of correlation between the experimental device and the numerical model, also revealing a linear trend with the input power. The maximum relative difference between the temperature measurements and simulations is 3%. The low standard deviation values presented in Table 3 prove the good reproducibility of the proposed experimental device and precise control of all variables.

The temperatures measured by ten thermocouples during the heating phase for the 400 W input power are shown in Figure 7. This reveals that a steady-state thermal regime is only achieved 300 s after starting the heating phase. It is also observed that the maximum temperature occurs at the interface between the insert and the heat sources. At the base of

the cutting insert is observed that the maximum temperature is close to 100 °C. As expected, the temperatures are higher for the thermocouples in direct contact with the cutting insert base (T3–T6), being slightly higher for the thermocouples near the heat sources (T3 and T4). It should be mentioned that similar temperature are observed between the two symmetry planes, i.e., {(T3 vs. T4), (T5 vs. T6), (T7 vs. T8), (T9 vs. T10)}, which demonstrates good balance in the heat flow introduced by the two heat sources and the symmetry of thermal contact resistance between the pair of components.

All these results allow to validate the implementation of the experimental device and support the performance of new studies to evaluate the heat transfer rate influence produced by the inclusion of micro-textures on the cutting insert surface.

3.4. Heat Transfer Rate Results and Discussion

The micro-textures effectiveness in promoting heat extraction is evaluated by comparing the heat transfer rate of the cutting inserts with and without micro-textures. The study involved four consecutive tests on three samples of each of the four insert models presented in Figure 6, corresponding to a total of forty-eight experimental measurements. All the tests were conducted for the input power level of 400 W, being measured the inlet T1 and outlet T2 temperatures and the mass flow rate of water after reaching the steady-state regime, see Figure 7. The respective heat transfer rate is evaluated according to Equation (1), by considering the mass flow rate of water, the temperature difference between inlet and outlet, and the constant specific heat of 4187 J/kg.K.

Table 4 presents the average and the standard deviation values of the temperatures T1 and T2, the respective temperature difference ΔT, the mass flow rate of water, and the heat transfer rate results per sample and insert model. Indeed, an increase in the heat transfer rate is observed with groove depth, corresponding to 0.92%, 2.58%, and 3.77% for Grid depth 1, Grid depth 2, and Grid depth 3, respectively. Similar values among the three samples for the same insert model are found. However, this is also followed by the increase in the respective standard deviation, which is associated with the higher dispersion of results within the same insert model. A possible explanation for this is the difference in the depth of the grooves between the samples. As already mentioned, these are created using laser ablation on green compacts. The amount of material removed will depend on the distance from the laser focal point to the compact green surface. The height of these compacts may vary slightly between samples and within the sample due to their manufacturing process and, therefore, grooves with different depths may be produced. This deduction results from the observation of the surface topology by scanning electron microscopy (SEM), which is shown in Figure 8 for the three different depths. The images reveal a non-uniform distribution of the depth of the grooves along the grid, which degrades with grooves depth. Furthermore, these compacts are post-dewaxed and sintered, which also contributes to cutting inserts geometric distortions [40]. These distortions were identified on the lateral faces of the cutting inserts, due to the increase of thermal contact resistance with heat sources. The problem was overcome by placing a thin layer of aluminum between the two elements.
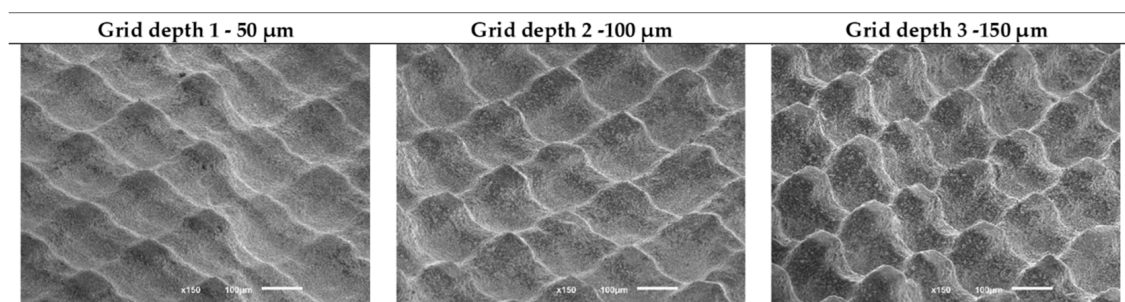

Figure 8. Images of surface topology by scanning electron microscopy.

Table 4. Experimental thermal results for different insert models.

Insert Model	Sample	T1 [°C]	T2 [°C]	ΔT [°C]	Mass Flow Rate [g/s]	Sample Heat Transfer Rate [W]	Insert Model Heat Transfer Rate [W]
Standard	1	15.96 ± 0.58	20.47 ± 0.60	4.51 ± 0.01	15.89 ± 0.0538	300.16 ± 1.36	
	2	15.90 ± 0.46	20.36 ± 0.46	4.46 ± 0.02	15.99 ± 0.0478	298.60 ± 0.84	299.20 ± 0.84
	3	16.65 ± 0.73	21.11 ± 0.72	4.46 ± 0.02	16.01 ± 0.0509	298.84 ± 0.69	
Grid depth 1 50 μm	1	15.36 ± 0.35	19.85 ± 0.35	4.49 ± 0.01	15.94 ± 0.0108	299.69 ± 0.39	
	2	14.19 ± 0.28	18.74 ± 0.29	4.55 ± 0.01	15.98 ± 0.0484	304.57 ± 0.42	302.07 ± 2.44
	3	16.95 ± 0.58	21.45 ± 0.56	4.50 ± 0.02	16.04 ± 0.0414	301.96 ± 0.58	
Grid depth 2 100 μm	1	14.49 ± 0.31	19.08 ± 0.30	4.60 ± 0.02	15.95 ± 0.0771	307.00 ± 1.28	
	2	15.33 ± 0.07	19.89 ± 0.06	4.55 ± 0.01	15.97 ± 0.0350	304.43 ± 0.89	306.91 ± 2.44
	3	18.05 ± 0.50	22.64 ± 0.48	4.58 ± 0.03	16.12 ± 0.0781	309.30 ± 0.76	
Grid depth 3 150 μm	1	14.53 ± 0.26	19.18 ± 0.28	4.66 ± 0.02	15.96 ± 0.0292	311.11 ± 1.36	
	2	15.69 ± 0.49	20.27 ± 0.48	4.58 ± 0.02	15.98 ± 0.0514	306.08 ± 0.12	310.49 ± 4.13
	3	14.76 ± 0.30	19.42 ± 0.29	4.66 ± 0.03	16.09 ± 0.0111	314.27 ± 0.54	

These results were only possible to obtain due to strict control of temperatures and the input power during the experimental tests. The measurement procedure allowed us to identify variations of less than 1% in the heat transfer rate.

These experimental results agree with the ones presented by other authors, that the inclusion of micro-textures leads to a decrease in the cutting insert temperature [16,20]. Furthermore, we can say that the contribution of microtextures to heat extraction is small compared to other tribological effects, such as the reduction of the contact area and the friction coefficient, which agrees with the findings presented by other authors [17,21,32].

4. Conclusions

This work presents an experimental device devoted to the quantification of the heat transfer rate from cutting inserts. It was designed to replicate the generation and transfer of heat that occurs during cutting operations, with the advantage of quantifying the single effect of micro-textures. The numerical study allowed us to optimize the linear response and the device sensitivity. A good correlation between preliminary experimental measurements and the numerical simulation was found, which allowed us to validate the implementation of the experimental device. The measurement procedure and the strict control of the different variables allowed to obtain results with good precision, which makes it possible to identify small variations in the heat transfer rate of less than 1% between cutting insert models. The insert surface micro-textures were introduced in the form of a square grid grooves of 100 μm × 100 μm, with depths of 50, 100, and 150 μm, by laser ablation in green compacts. The experimental results show a progressive increase in heat transfer rate with the depth of the groove, being the highest of 3.77% for the depth of 150 μm. This improvement is justified by the increase in the surface-to-coolant contact area, the generation of a higher turbulent flow of the fluid near the cutting insert surface, and the rise in the surface wettability. Based on these findings, we can say that the micro-textures lead to a slight increase in the heat dissipation of the cutting inserts, although, their contribution to tools' overall performance is smaller compared to other tribological effects. Additional studies will be conducted to investigate micro-textures with other geometries to further improve heat extraction. The influence of surface coatings will be another important research line.

Author Contributions: Conceptualization, J.R., H.L., O.C.P., B.G., G.M. and F.S.S.; methodology, J.R., H.L. and O.C.P.; investigation, J.R., H.L. and P.A.G.P.; writing—original draft preparation, J.R. and H.L.; writing—review and editing, J.R., H.L., O.C.P., B.G., P.A.G.P., G.M. and F.S.S.; supervision, H.L. and O.C.P. All authors have read and agreed to the published version of the manuscript.

Conflicts of Interest: The authors declare no conflict of interest.

References

1. Kamperidou, V.; Barboutis, I. *Lathe Tool—It's Development from the Ancient Times to Nowadays*; Faculty of Forestry, Zagreb University: Zagreb, Croatia, 2013; pp. 57–64.
2. Tamil Alagan, N.; Zeman, P.; Hoier, P.; Beno, T.; Klement, U. Investigation of micro-textured cutting tools used for face turning of alloy 718 with high-pressure cooling. *J. Manuf. Process.* **2019**, *37*, 606–616. [CrossRef]
3. Alagan, N.T.; Beno, T.; Hoier, P.; Klement, U.; Wretland, A. Influence of surface features for increased heat dissipation on tool wear. *Materials* **2018**, *11*, 664. [CrossRef]
4. Alagan, N.T.; Beno, T.; Wretland, A. Investigation of Modified Cutting Insert with Forced Coolant Application in Machining of Alloy 718. *Procedia CIRP* **2016**, *42*, 481–486. [CrossRef]
5. Panigrahi, R.R.; Panda, A.; Sahoo, A.K.; Kumar, R. Machining performance measures of high temperature heat resistant super alloys: A review. *Mater. Today Proc.* **2019**, *18*, 4524–4530. [CrossRef]
6. Singh, J.; Gill, S.S.; Dogra, M.; Singh, R. A review on cutting fluids used in machining processes. *Eng. Res. Express* **2021**, *3*, 012002. [CrossRef]
7. Obikawa, T.; Kamata, Y.; Asano, Y.; Nakayama, K.; Otieno, A.W. Micro-liter lubrication machining of Inconel 718. *Int. J. Mach. Tools Manuf.* **2008**, *48*, 1605–1612. [CrossRef]
8. Chiou, R.Y.; Lu, L.; Chen, J.S.J.; North, M.T. Investigation of dry machining with embedded heat pipe cooling by finite element analysis and experiments. *Int. J. Adv. Manuf. Technol.* **2007**, *31*, 905–914. [CrossRef]
9. Vicentin, G.C.; Sanchez, L.E.A.; Scalon, V.L.; Abreu, G.G.C. A sustainable alternative for cooling the machining processes using a refrigerant fluid in recirculation inside the toolholder. *Clean Technol. Environ. Policy* **2011**, *13*, 831–840. [CrossRef]
10. Sharma, V.S.; Dogra, M.; Suri, N.M. Cooling techniques for improved productivity in turning. *Int. J. Mach. Tools Manuf.* **2009**, *49*, 435–453. [CrossRef]
11. Sun, X.; Bateman, R.; Cheng, K.; Ghani, S.C. Design and analysis of an internally cooled smart cutting tool for dry cutting. *Proc. Inst. Mech. Eng. Part B J. Eng. Manuf.* **2012**, *226*, 585–591. [CrossRef]
12. Sugihara, T.; Tanaka, H.; Enomoto, T. Development of Novel CBN Cutting Tool for High Speed Machining of Inconel 718 Focusing on Coolant Behaviors. *Procedia Manuf.* **2017**, *10*, 436–442. [CrossRef]
13. Feng, Y.; Zhang, J.; Wang, L.; Zhang, W.; Tian, Y.; Kong, X. Fabrication techniques and cutting performance of micro-textured self-lubricating ceramic cutting tools by in-situ forming of Al2O3-TiC. *Int. J. Refract. Met. Hard Mater.* **2017**, *68*, 121–129. [CrossRef]
14. Sharma, V.; Pandey, P.M. Recent advances in turning with textured cutting tools: A review. *J. Clean. Prod.* **2016**, *137*, 701–715. [CrossRef]
15. Ribeiro, F.S.F.; Lopes, J.C.; Bianchi, E.C.; de Angelo Sanchez, L.E. Applications of texturization techniques on cutting tools surfaces—A survey. *Int. J. Adv. Manuf. Technol.* **2020**, *109*, 1117–1135. [CrossRef]
16. Enomoto, T.; Sugihara, T.; Yukinaga, S.; Hirose, K.; Satake, U. Highly wear-resistant cutting tools with textured surfaces in steel cutting. *CIRP Ann. Manuf. Technol.* **2012**, *61*, 571–574. [CrossRef]
17. Machado, A.R.; da Silva, L.R.R.; de Souza, F.C.R.; Davis, R.; Pereira, L.C.; Sales, W.F.; de Rossi, W.; Ezugwu, E.O. State of the art of tool texturing in machining. *J. Mater. Process. Technol.* **2021**, *293*, 117096. [CrossRef]
18. Sugihara, T.; Enomoto, T. Improving anti-adhesion in aluminum alloy cutting by micro stripe texture. *Precis. Eng.* **2012**, *36*, 229–237. [CrossRef]
19. Chen, Y.; Wang, J.; Chen, M. Enhancing the machining performance by cutting tool surface modifications: A focused review. *Mach. Sci. Technol.* **2019**, *23*, 477–509. [CrossRef]
20. Liao, Z.; Xu, D.; Axinte, D.; M'Saoubi, R.; Thelin, J.; Wretland, A. Novel cutting inserts with multi-channel irrigation at the chip-tool interface: Modelling, design and experiments. *CIRP Ann.* **2020**, *69*, 65–68. [CrossRef]
21. Fang, S.; Herrmann, T.; Rosenkranz, A.; Gachot, C.; Marro, F.G.; Mücklich, F.; Llanes, L.; Bähre, D. Tribological Performance of Laser Patterned Cemented Tungsten Carbide Parts. *Procedia CIRP* **2016**, *42*, 439–443. [CrossRef]
22. Guimarães, B.; Silva, J.; Fernandes, C.M.; Figueiredo, D.; Carvalho, O.; Miranda, G.; Silva, F.S. Understanding drop spreading behaviour on WC-10wt%Co cutting tools—An experimental and numerical study. *Colloids Surf. A Physicochem. Eng. Asp.* **2022**, *637*, 128268. [CrossRef]
23. Guimarães, B.; Fernandes, C.M.; Figueiredo, D.; Carvalho, O.; Silva, F.S.; Miranda, G. Effect of laser surface texturing on the wettability of WC-Co cutting tools. *Int. J. Adv. Manuf. Technol.* **2020**, *111*, 1991–1999. [CrossRef]

24. Pang, M.; Liu, X.; Liu, K. Effect of wettability on the friction of a laser-textured cemented carbide surface in dilute cutting fluid. *Adv. Mech. Eng.* **2017**, *9*, 1–9. [CrossRef]

25. Zhao, Y.; Lu, Q.; Li, M.; Li, X. Anisotropic Wetting Characteristics on Submicrometer-Scale Periodic Grooved Surface. *Langmuir* **2007**, *23*, 6212–6217. [CrossRef]

26. Özel, T.; Biermann, D.; Enomoto, T.; Mativenga, P. Structured and textured cutting tool surfaces for machining applications. *CIRP Ann.* **2021**, *70*, 495–518. [CrossRef]

27. Zhang, K.; Deng, J.; Xing, Y.; Li, S.; Gao, H. Effect of microscale texture on cutting performance of WC/Co-based TiAlN coated tools under different lubrication conditions. *Appl. Surf. Sci.* **2015**, *326*, 107–118. [CrossRef]

28. Lei, S.; Devarajan, S.; Chang, Z. A study of micropool lubricated cutting tool in machining of mild steel. *J. Mater. Process. Technol.* **2009**, *209*, 1612–1620. [CrossRef]

29. Kawasegi, N.; Sugimori, H.; Morimoto, H.; Morita, N.; Hori, I. Development of cutting tools with microscale and nanoscale textures to improve frictional behavior. *Precis. Eng.* **2009**, *33*, 248–254. [CrossRef]

30. Sugihara, T.; Enomoto, T. Development of a cutting tool with a nano/micro-textured surface—Improvement of anti-adhesive effect by considering the texture patterns. *Precis. Eng.* **2009**, *33*, 425–429. [CrossRef]

31. Sakkaki, M.; Sadegh Moghanlou, F.; Vajdi, M.; Pishgar, F.; Shokouhimehr, M.; Shahedi Asl, M. The effect of thermal contact resistance on the temperature distribution in a WC made cutting tool. *Ceram. Int.* **2019**, *45*, 22196–22202. [CrossRef]

32. Kim, D.M.; Lee, I.; Kim, S.K.; Kim, B.H.; Park, H.W. Influence of a micropatterned insert on characteristics of the tool–workpiece interface in a hard turning process. *J. Mater. Process. Technol.* **2016**, *229*, 160–171. [CrossRef]

33. Fang, Z.; Obikawa, T. Influence of cutting fluid flow on tool wear in high-pressure coolant turning using a novel internally cooled insert. *J. Manuf. Process.* **2020**, *56*, 1114–1125. [CrossRef]

34. Kitagawa, T.; Kubo, A.; Maekawa, K. Temperature and wear of cutting tools in high-speed machining of Inconel 718 and Ti-6Al-6V-2Sn. *Wear* **1997**, *202*, 142–148. [CrossRef]

35. Shu, S.; Cheng, K.; Ding, H.; Chen, S. An Innovative Method to Measure the Cutting Temperature in Process by Using an Internally Cooled Smart Cutting Tool. *J. Manuf. Sci. Eng.* **2013**, *135*, 061018. [CrossRef]

36. Yao, B.; Sun, W.; Chen, B.; Yu, X.; He, Y.; Feng, W.; Wang, S. An Independent Internal Cooling System for Promoting Heat Dissipation during Dry Cutting with Numerical and Experimental Verification. *Appl. Sci.* **2017**, *7*, 332. [CrossRef]

37. Yang, K.; Liang, Y.-C.; Zheng, K.-N.; Bai, Q.-S.; Chen, W.-Q. Tool edge radius effect on cutting temperature in micro-end-milling process. *Int. J. Adv. Manuf. Technol.* **2011**, *52*, 905–912. [CrossRef]

38. Longbottom, J.M.; Lanham, J.D. Cutting temperature measurement while machining—A review. *Aircr. Eng. Aerosp. Technol.* **2005**, *77*, 122–130. [CrossRef]

39. Komanduri, R.; Hou, Z.B. A review of the experimental techniques for the measurement of heat and temperatures generated in some manufacturing processes and tribology. *Tribol. Int.* **2001**, *34*, 653–682. [CrossRef]

40. Ranjan, P.; Hiremath, S.S. Role of textured tool in improving machining performance: A review. *J. Manuf. Process.* **2019**, *43*, 47–73. [CrossRef]

41. Çengel, Y.A.; Ghajar, A.J. *Heat and Mass Transfer Fundamentals & Applications*, 5th ed.; McGraw-Hill Education: New York, NY, USA, 2015; p. 1208.

42. Kataria, R.; Kumar, J. Machining of WC-Co Composites—A Review. *Mater. Sci. Forum* **2015**, *808*, 51–64. [CrossRef]

43. Guimarães, B.; Figueiredo, D.; Fernandes, C.M.; Silva, F.S.; Miranda, G.; Carvalho, O. Laser machining of WC-Co green compacts for cutting tools manufacturing. *Int. J. Refract. Met. Hard Mater.* **2019**, *81*, 316–324. [CrossRef]